Iranian Journal of Science & Technology, Transaction B, Engineering, Vol. 33, No. B1, pp 31-48
Printed in The Islamic Republic of Iran, 2009


# A CONSTITUTIVE MODEL FOR SAND LIQUEFACTION UNDER ROTATIONAL SHEAR*

A. LASHKARI

Dept. of Civil Engineering, Faculty of Engineering, Islamic Azad University of Shiraz, Shiraz, I. R. of Iran
Email: Lashkari_ali@hamyar.net

**Abstract–** Recently, the undrained anisotropic behavior of sand subjected to rotational shear has been a subject of great interest in both fields of experimental studies and constitutive modeling. Herein, based on the critical state concept and the bounding surface plasticity framework, a unified sand model is presented that is able to simulate the liquefaction of sand subjected to various stress paths, especially rotational shear. Using two anisotropy state parameters, the effect of soil anisotropy on the location of critical state line, dilatancy, plastic modulus, and flow direction is considered in constitutive equations. Finally, the simulative capability of the presented model is illustrated by comparison with the experimental data reported by independent research teams over a wide range of densities, stress paths, and stress levels.

**Keywords–** Liquefaction, rotational shear, principal stress axes, bounding surface, anisotropy, sand

## 1. INTRODUCTION

The mechanical behavior of granular soils is affected by numerous factors. Among them, density, current mean principal effective stress, manner of deposition, and shearing mode are much more significant than the others [1-11]. Due to the effect of the gravity field acting on grains during deposition, fabric of granular soils becomes inherently anisotropic. As a result, the mechanical behavior of soil depends highly on the orientation of the applied shear. For example, while sand may exhibit a very dilative behavior in triaxial compression, it may also exhibit very contractive behavior and fail due to flow liquefaction under triaxial extension [6, 10]. Historically, most of the existing experimental studies have been conducted under the fixed direction of the principal stress axes by using triaxial or simple shear devices. Using a hollow cylindrical apparatus, Ishihara and Towhata [3] studied sand behavior subjected to rotational shear. Rotational shear, also known in the literature as continuous rotation of principal stress axes, is a pattern of loading in which the rotation of principal stress axes takes place under a constant amount of shear stress. The state of shear stress acting on seabed deposits by passing waves, traffic loads on the subgrade of pavements, and earthquake induced loadings are common examples of the rotational shear [3, 11]. Figure 1 shows the deviatoric stress path of the rotational shear where $\sigma_{11}, \sigma_{33}, \sigma_{13}$ and $\sigma_{22}$ are vertical, horizontal, shear, and radial components of the stress tensor acting on an infinite small element of soil (Fig. 2). Moreover, $\sigma_1, \sigma_2$, and $\sigma_3$ are major, intermediate, and minor principal stresses, respectively. Rotation of principal stress axes occurs in $\sigma_1 - \sigma_3$ plane and thus, $\sigma_{22} = \sigma_2$. In the experiments of Ishihara and Towhata [3], drainage was not allowed. The major finding they reported was that even though the magnitude of applied shear stress is kept unchanged, the rotational shear always results in pore pressure build up, and can eventually lead to liquefaction. More recently, Nakata et al. [9] and Yang et al.

*Received by the editors February 5, 2008; Accepted June 25, 2008.

[11] studied the behavior of sand of various densities subjected to rotational shear and confirmed the findings of Ishihara and Towhata [3].

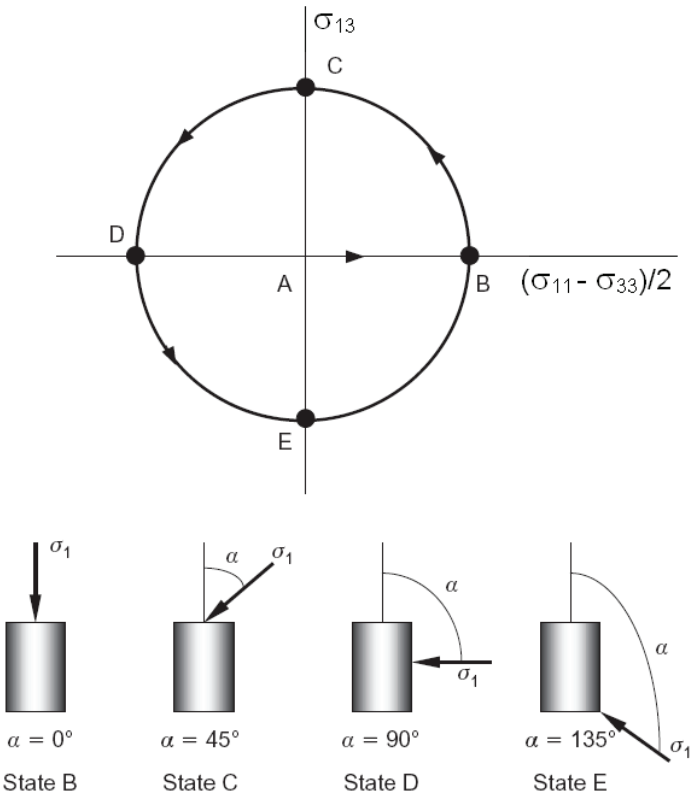


Fig. 1. Stress path of rotational shear in deviator plane

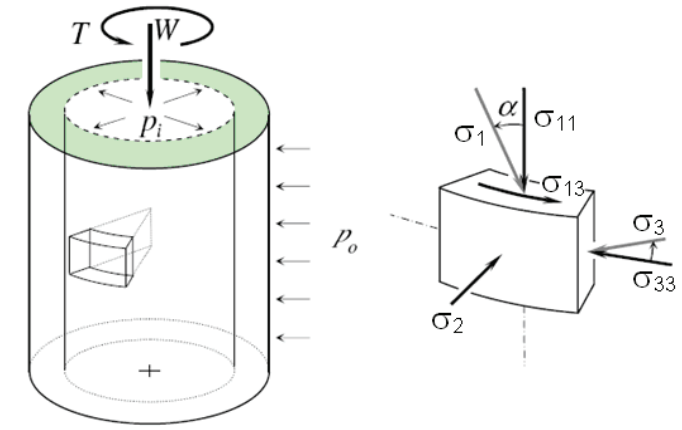


Fig. 2. External forces and associate stress components acting on infinite small element of soil in hollow cylindrical apparatus

Except for the past few years, sand behavior during rotational shear has been neither well addressed, nor well considered in the establishment of constitutive equations. Using an infinite number of non-linear springs, Towhata and Ishihara [12] proposed a constitutive model for rotational shear. Gutierrez et al. [13] suggested a nested yield surface model for sand non-coaxial flow during rotational shear. Sassa and Sekiguchi [14] considered rotational shear by imposing modifications to the generalized plasticity framework of Pastor et al. [15]. Considering the possibility of rotational hardening, Tsutsumi and Hashiguchi [16] proposed a sophisticated sub-loading surface model capable of simulating sand behavior during the continuous rotation of principal stresses. It is worth noting that in two-dimensional case, the

latter approach is very similar to Gutierrez et al. [13]. In multi-plane framework, Chang and Sture [17] and Sadrnejad [18] considered anisotropy in their constitutive models. Using an anisotropy state parameter, Li and Dafalias [19] introduced a bounding surface hypoplasticity model for simulation of anisotropic behavior of sand subjected to shear when the direction of principal stress was kept unchanged during loading. It should be mentioned that anisotropy state parameters are usually joint invariants of stress, stress rate, plastic strain and fabric tensors. Recently, Li and Dafalias [20] extended their previous work to account for rotational shear by introducing an additional plastic mechanism. More recently, using two anisotropy state parameters, Lashkari and Latifi [21-23] proposed a bounding surface hypoplaticity model for the non-coaxial flow of sand. The latter approach is successfully capable of considering the effect of soil anisotropy on the location of critical state line, dilatancy, plastic modulus, and flow direction under various stress paths and patterns of loading.

In this study, several improvements have been made on Lashkari and Latifi's model [23]. A new aspect, modified plastic modulus and dilatancy rule, are employed in the present framework, which are more accurate under multitude cycles of principal stress rotation. Moreover, the number of model parameters is less than that in the predecessor framework that facilitates the model calibration. This work ends in a complete set of model evaluation *versus* experimental data of sand behavior under drastically different undrained stress paths including rotational shear, which were not considered in the original framework.

## 2. GENERAL FORMULATION OF MODEL

The model is formulated in Ishihara's three-dimensional stress and strain spaces. In the mentioned stress and strain spaces, two components have shear nature and one is spherical. The assumed configuration of the stress field is identical with the most general pattern of loading acting on an infinite small element of soil in a hollow cylindrical apparatus. Components of the new stress space are defined as

$$\begin{aligned} X &= \frac{\sigma_{11} - \sigma_{33}}{2} \\ Y &= \sigma_{13} \\ p &= \frac{1}{3}(\sigma_1 + \sigma_2 + \sigma_3) \end{aligned} \tag{1}$$

where X and Y are shear stress components and p is mean principal effective stress. Similarly, components of the new strain space can be defined as:

$$\begin{aligned} \varepsilon_X &= \frac{\varepsilon_{11} - \varepsilon_{33}}{2} \\ \varepsilon_Y &= \varepsilon_{13} \\ \varepsilon_v &= \varepsilon_1 + \varepsilon_2 + \varepsilon_3 \end{aligned} \tag{2}$$

where $\varepsilon_X$ and $\varepsilon_Y$ are components of shear strain along X and Y directions, and $\varepsilon_v$ is volumetric strain.

It is assumed that each strain rate can be decomposed into elastic (recoverable) and plastic (irrecoverable) parts as:

$$\begin{aligned} \dot{\varepsilon}_X &= \dot{\varepsilon}_X^e + \dot{\varepsilon}_X^p \\ \dot{\varepsilon}_Y &= \dot{\varepsilon}_Y^e + \dot{\varepsilon}_Y^p \\ \dot{\varepsilon}_v &= \dot{\varepsilon}_v^e + \dot{\varepsilon}_v^p \end{aligned} \tag{3}$$

In the above equations, superscripts e and p denote the elastic and plastic parts of strain rate. Note that the dot sign indicates the rate of parameters.

The generalized isotropic form of the Hooke's law is used for elasticity. This law, re-written in X-Y-p and $\varepsilon_X$-$\varepsilon_Y$-$\varepsilon_v$ spaces, is in the following form:

$$\begin{aligned} \dot{X} &= 2G\ \dot{\varepsilon}_X^e \\ \dot{Y} &= 2G\ \dot{\varepsilon}_Y^e \\ \dot{p} &= K\ \dot{\varepsilon}_v^e \end{aligned} \tag{4}$$

In the above equations, G and K are respectively the elastic shear and bulk moduli that are calculated by the following empirical relationships [24]:

$$\begin{aligned} G &= G_0\ p_{ref}\ \frac{(2.973-e)^2}{1+e}\sqrt{\frac{p}{p_{ref}}} \\ K &= \frac{2}{3}G\left(\frac{1+\nu}{1-2\nu}\right) \end{aligned} \tag{5}$$

where $\nu$ is Poisson ratio. Both $G_0$ and $\nu$ are the model parameters and $p_{ref}$ is a reference pressure that can be taken as atmospheric pressure (i.e., 101 kPa).

In the plasticity theory, components of the plastic strain rate can be calculated by:

$$\begin{aligned} \dot{\varepsilon}_X^p &= \Lambda\ R_X \\ \dot{\varepsilon}_Y^p &= \Lambda\ R_Y \\ \dot{\varepsilon}_v^p &= \Lambda\ D \end{aligned} \tag{6}$$

$\Lambda$ in Eqs. (6), so-called loading index, is the magnitude of vector $\vec{\Lambda}$ that is the projection of plastic strain rate vector on X-Y plane (Fig. 3). Besides, $R_X$ and $R_Y$ are components of the unit vector $\vec{R}\ (=\vec{\Lambda}/\Lambda = R_X\ \vec{e}_X + R_Y\ \vec{e}_Y)$ along X and Y directions where $\vec{e}_X$ and $\vec{e}_Y$ are the unit vectors of the X and Y axes. Finally, D is the dilatancy function that represents the coupling effect between plastic volumetric and shear strains as a result of shear stress. Loading index is calculated by:

$$\Lambda = \left\langle \frac{\dot{X}\ n_X + \dot{Y}\ n_Y + \dot{p}\ n_p}{K_p} \right\rangle \tag{7}$$

where $\langle\ \rangle$ are Macauley brackets. For a given scalar value parameter x, $\langle x\rangle = x$ if $x > 0$, otherwise $\langle x\rangle = 0$. In the absence of yield surface (see section 3), yield vector is defined along the stress rate vector. Based on this, $n_X(=\dot{X}/\sqrt{\dot{X}^2+\dot{Y}^2})$, $n_Y(=\dot{Y}/\sqrt{\dot{X}^2+\dot{Y}^2})$, and $n_p(=-(X\ n_X + Y\ n_Y)/p)$ are components of the yield vector, $\vec{n}\ (=n_X\ \vec{e}_X + n_Y\ \vec{e}_Y + n_p\ \vec{e}_p)$, along X, Y, and p directions. Finally, $K_p$ is plastic modulus.

Using Eqs. (1), (6), and (7), loading index can be calculated by:

$$\Lambda = \frac{2G(n_X\ \dot{\varepsilon}_X + n_Y\ \dot{\varepsilon}_Y) + Kn_p\dot{\varepsilon}_v}{K_p + 2G(R_X n_X + R_Y n_Y) + KDn_p} \tag{8}$$

Hence, considering Eqs. (4) and (6), one can express the stress increments by:

$$\dot{X} = 2G\left(\dot{\varepsilon}_X - \left\langle \frac{2G(n_X\,\dot{\varepsilon}_X + n_Y\,\dot{\varepsilon}_Y) + Kn_p\dot{\varepsilon}_v}{K_p + 2G(R_X n_X + R_Y n_Y) + KDn_p} \right\rangle R_X\right)$$
$$\dot{Y} = 2G\left(\dot{\varepsilon}_Y - \left\langle \frac{2G(n_X\,\dot{\varepsilon}_X + n_Y\,\dot{\varepsilon}_Y) + Kn_p\dot{\varepsilon}_v}{K_p + 2G(R_X n_X + R_Y n_Y) + KDn_p} \right\rangle R_Y\right) \qquad (9)$$
$$\dot{p} = K\left(\dot{\varepsilon}_v - \left\langle \frac{2G(n_X\,\dot{\varepsilon}_X + n_Y\,\dot{\varepsilon}_Y) + Kn_p\dot{\varepsilon}_v}{K_p + 2G(R_X n_X + R_Y n_Y) + KDn_p} \right\rangle D\right)$$

For completeness of the model formulation, one must specify the particular definition of $\vec{R}$, D, and $K_p$. These terms are defined in section 4.

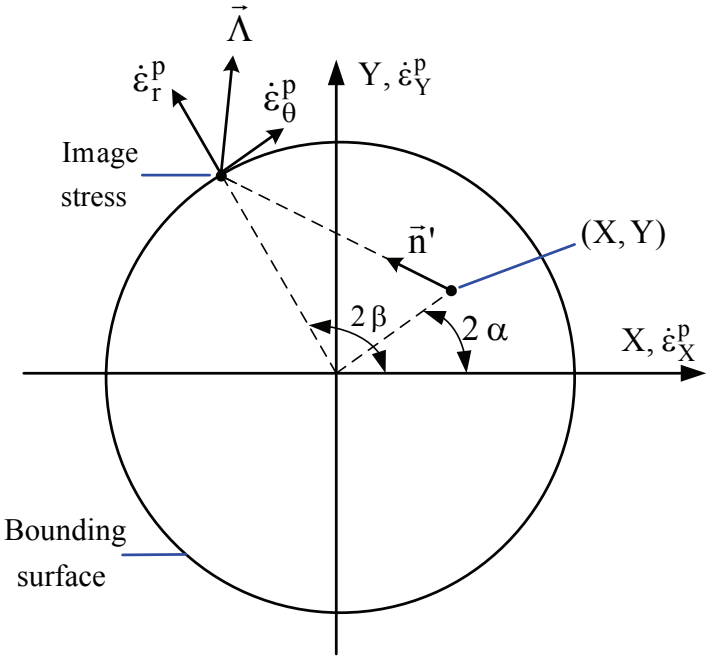


Fig. 3. Schematic illustration of the model flow rule in X-Y plane

## 3. BOUNDING SURFACE

The model is formulated in bounding surface plasticity framework [25, 26]. Bounding surface defines the domain of permissible stress states. No yield surface or domain of pure elasticity is introduced in the model. The latter assumption is supported by a number of experimental studies on the behavior of granular media [27-29].

When sand is subjected to rotation of principal stress axes, bounding surface can be defined in the following form [23]:

$$\sqrt{X^2 + Y^2} - \frac{1}{2}M_b\,p = 0 \qquad (10)$$

where,

$$M_b = \frac{M_c\,g(b,c)\exp(-n\psi)}{\sqrt{b^2 - b + 1}} \qquad (11)$$

where $M_b$ defines the bounding surface size and $M_c$ is the slope of critical state line in shear stress *versus* mean principal effective stress plane measured in the compression mode of the triaxial. Parameter c equals

the ratio $M_e/M_c$ in which $M_e$ is the slope of critical state line in the triaxial extension. $b\,(=(\sigma_2-\sigma_3)/(\sigma_1-\sigma_3))$ is the coefficient of intermediate principal effective stress. b varies between 0 and 1 corresponding to triaxial compression and extension, respectively. g(b,c) is an appropriate interpolation function which simulates the actual shape of bounding surface. A slightly modified form of the interpolation function of Gudehus [30] is adopted here:

$$g(b,c)=\frac{4c}{2(1+c)-(1-c)\dfrac{(1+b)(2b^2-5b+2)}{(b^2-b+1)^{\frac{3}{2}}}} \tag{12}$$

g(b,c) has two boundaries of 1 and c corresponding to the compression and extension modes of the triaxial. Note that the model does not depend on a specific interpolation function and any other interpolation functions can be used instead of Eq. (12). $\psi\,(=e-e_c)$ is the state parameter of Been and Jefferies [1], where $e_c$ is the critical void ratio measured in the current amount of mean principal effective stress. According to Li and Dafalias [31], the term $\exp(-n\psi)$ is introduced to Eq. (11) to consider the effect of soil state on bounding surface size. In Eq. (11), $M_c$, c, and n are model parameters.

## 4. ANISOTROPIC BEHAVIOR OF GRANULAR SOILS

Anisotropy of a granular medium is usually expressed by a second order fabric tensor. In nature, granular soils are nearly transversely isotropic. For this case, one can define a fabric tensor in the following form [32]:

$$\mathbf{F}=\frac{1}{2}\begin{pmatrix}2a & 0 & 0\\ 0 & 1-a & 0\\ 0 & 0 & 1-a\end{pmatrix} \tag{13}$$

where a is a micromechanical based model parameter which describes the preferred orientation of grains in a granular mass. In the case of isotropy, a=1/3, when all grains are oriented toward the vertical direction, a=1. In practical cases, it is expected that $0<a<1/3$.

Since the model has been formulated in transformed stress and strain spaces, it is logical to introduce a similar transformed space for fabric. Lashkari & Latifi [22, 23] introduced the concept of fabric vector, $\vec{F}$, as another representation of anisotropy within a granular mass:

$$\vec{F}=F_X\,\vec{e}_X+F_Y\,\vec{e}_X \tag{14}$$

where

$$\begin{aligned}F_X&=\frac{F_{11}-F_{33}}{2}\\ F_Y&=F_{13}\end{aligned} \tag{15}$$

The original purpose of the fabric tensor concept is to define deviation from isotropy. Thus, the introduction of a spherical component for the fabric vector is neither meaningful nor fruitful.

It has been observed experimentally that the anisotropic response of granular masses depends on the direction of the current applied loading and principal stresses with respect to the plane of deposition [6-10]. Lashkari [33] and Lashkari & Latifi [23] stated that at least two anisotropy state parameters are required for reasonable constitutive modeling of strength, dilatancy, and non-coaxial flow of sand:

$$\begin{aligned} A &= \vec{F} \cdot \vec{n}' \\ B &= \vec{F} \cdot \vec{\Theta} \end{aligned} \tag{16}$$

where A and B are anisotropy state parameters. $\vec{n}' (= n_X \vec{e}_X + n_Y \vec{e}_Y)$ is the projection of $\vec{n}$ on the X-Y plane. $\vec{\Theta} (= \cos 2\alpha \ \vec{e}_X + \sin 2\alpha \ \vec{e}_Y)$ is a unit vector defining the direction of major principal effective stress in X-Y plane.

## 5. ACCOUNTING FOR FABRIC ANISOTROPY IN CONSTITUTIVE EQUATIONS

Each of the anisotropy state parameters introduced in the previous section is able to partly consider the interaction between loading/fabric of anisotropic soil. Thus, in order to develop a constitutive model capable of accounting for the anisotropic behavior of sand, the direction of the plastic flow, plastic modulus, and the location of the critical state line are defined using these anisotropy state parameters in the following sub-sections.

### *a) Direction of plastic strain rate*

Sands generally exhibit non-coaxial flow when subjected to rotation of principal stress axes. The mentioned non-coaxiality is much higher under rotational shear. Lashkari and Latifi [21-23] proposed a flow rule that is reasonably able to predict flow direction under various stress paths during the rotation of principal stress axes. This flow rule is adopted here:

$$\begin{aligned} R_X &= \frac{1}{\sqrt{1+f^2}} \left( \cos 2\beta - f \sin 2\beta \right) \\ R_Y &= \frac{1}{\sqrt{1+f^2}} \left( f \cos 2\beta + \sin 2\beta \right) \end{aligned} \tag{17}$$

In above equation, $2\beta$ is the angle that the line connecting origin to image stress makes with the positive direction of the X-axis (Fig. 3). In this work, image stress is defined as where the extension the stress rate from the current state of stress crosses the bounding surface. At the image stress, $\vec{\Lambda}$ can be decomposed into radial, $\dot{\varepsilon}_r^p$, and tangential, $\dot{\varepsilon}_\theta^p$, components with respect to bounding surface (Fig. 3). Using this decomposition, the function f, non-coaxiality function, is defined as [21-23, 33]:

$$f = \frac{\dot{\varepsilon}_\theta^p}{\dot{\varepsilon}_r^p} \tag{18}$$

where:

$$f = -f_0 \ A \left( 1 - \frac{\eta}{M_b} \right) \sin 2\beta \tag{19}$$

in which $\eta (= (\sigma_1 - \sigma_3)/p)$ is stress ratio and $f_0$ is a model parameter.

### *b) Plastic modulus*

According to Vardoulakis and Georgopoulos [34], radial and rotational shear define two extremes of loading. Similar to the mentioned study, a manner of loading is classified as radial when $\vec{n}' \cdot \vec{\Theta} = \pm 1$. On the other hand, rotational shear takes place when $\vec{n}' \cdot \vec{\Theta} = 0$. The model plastic modulus has two distinct rules under radial and rotational shear as:

$$K_p^1 = H_1(1 - H_3\, e)\, G\left(\frac{M_b}{\eta} - 1\right) C_1(k_1, \alpha) \tag{20}$$

$$K_p^2 = H_2(1 - H_3\, e)\, G\left(1 - \frac{\eta}{M_b}\right)^{\kappa} C_1(k_2, \alpha)\, C_2(\varepsilon_v^p) \tag{21}$$

Where $K_p^1$ and $K_p^2$ are the rules of plastic modulus under radial and rotational shear, respectively. $H_1$, $H_2$, $H_3$, $k_1$ (for radial loading), $k_2$ (for rotational shear), and $\kappa$ are model parameters. In order to consider the effect of anisotropy of granular masses on plastic modulus, the term $C_1(k_i, \alpha)$ is added to rules of plastic modulus as:

$$C_1(k_i, \alpha) = \frac{1}{2}(1 + k_i) + \frac{1}{2}(1 - k_i)\cos\pi\left(\frac{B_c - B}{B_c - B_e}\right) \qquad i = 1,2 \tag{22}$$

where $B_c$ (=$F_X$) and $B_e$ (= - $F_X$) are the amounts of B (Eq. 16b) under the compression and extension modes of the triaxial, respectively. During rotation of principal stress axes, sand behavior is contractive [3, 9, 11, 35]. This phenomenon results in a pattern of densification. In Eq. (21), the term $C_2(\varepsilon_v^p)$ is added to account for the mentioned densification effect:

$$C_2(\varepsilon_v^p) = \begin{cases} 1 & N = 1 \\ \exp\left[\chi(\varepsilon_v^p - \varepsilon_{vo}^p)\right] & N > 1 \end{cases} \tag{23}$$

In Eq. (23), N is the number of principal stress axes rotation cycles, $\varepsilon_{vo}^p$ is the amount of volumetric plastic strain accumulated in the first cycle of principal stress axes rotation, and $\chi$ is a model parameter.

For a general pattern of loading $K_p$, plastic modulus, is obtained from the following rule:

$$\frac{1}{K_p} = \frac{1}{K_p^2} + \left(\frac{1}{K_p^1} - \frac{1}{K_p^2}\right)(\vec{n}' \cdot \vec{\Theta})^2 \tag{24}$$

***c) Dilatancy***

Similar to plastic modulus, a dilatancy function with two distinct rules under radial and rotational shear is proposed here as:

$$D^1 = D_1(M_d - nc\,\eta) \tag{25}$$

$$D^2 = \frac{D_2}{C_2(\varepsilon_v^p)}\left(\frac{M_c\, g(b,c)}{\sqrt{b^2 - b + 1}} - nc\,\eta\right) \tag{26}$$

In Eqs. (25-26), $D_1$ and $D_2$ are model parameters. $M_d$ is the phase transformation stress ratio at which contraction turns into dilation or *vise versa* [36]. $M_d$ varies as a function of soil state [1, 4]. To consider this effect and based on the work of Li and Dafalias [31], $M_d$ is defined as follows:

$$M_d = \frac{M_c\, g(b,c)\exp(m\psi)}{\sqrt{b^2 - b + 1}} \tag{27}$$

where m is a model parameter.

Both $M_b$ (Eq. 10) and $M_d$ (Eq. (25) depend on state parameter, $\psi$, which employs the soil critical state line. Various experimental evidence exist stating the dependence of the location of critical state line on soil anisotropy, and as a result, the pattern of loading [6, 7, 37, 38]. Based on the Dafalias et al. [39]

proposition, the following definition is used to consider the effect of anisotropy on the location of the critical state line:

$$e_c = e_\tau - \lambda\left(\frac{p}{p_{ref}}\right)^{\xi} \tag{28}$$

in which

$$e_\tau = e_A \exp(-A) \tag{29}$$

where $e_A$, $\lambda$ , and $\xi$ are model parameters.

In Eqs. (25-26), nc is the Gutierrez-Ishihara coefficient of dilatancy which considers the effect of non-coaxial flow on dilatancy [13, 40]:

$$nc = \cos 2(\omega - \alpha) \tag{30}$$

where $\omega$ is the angle that major principal plastic strain rate, $\dot{\varepsilon}_1^p$, makes with the vertical direction. Due to the possibility of non-coaxial flow in a general stress path, $\omega$ does not necessarily equal $\alpha$.

Similar to Eq. (24), dilatancy, D, is obtained from the following rule for a general pattern of loading:

$$D = D^2 + \left(D^1 - D^2\right)(\vec{n}' \cdot \vec{\Theta})^2 \tag{31}$$

## 6. THE MODEL EVALUATION

In this section, the presented model is evaluated *versus* the experimental data. In Japan in particular, many research groups conducted their experiments on Toyoura sand. As a result, a comprehensive and reliable set of experiments on the behavior of Toyoura sand under various stress paths, drainage conditions, and preparation methods now exist. Physical properties of Toyoura sand are listed in Table 1.

Table 1. Physical properties of Toyoura sand

| Mean diameter, $D_{50}$ (mm) | Uniformity coefficient, $U_c$ | Maximum void ratio, $e_{max}$ | Minimum void ratio, $e_{min}$ | Specific gravity, $G_s$ | Mineralogy | Angularity |
|---|---|---|---|---|---|---|
| 0.17- 0.23 § | 1.32 | 0.977 | 0.597 | 2.65 | 75 % quartz; 25 % feldespar | subangular |

§: 0.17 was reported by Verdugo and Ishihara [4] and Yoshimine et al. [6]; 0.23 was reported by Yang et al. [11]

Before the model evaluation, the model calibration process is outlined here. The presented model has 20 parameters in total. $G_0$ and $\nu$ are related to the elastic branch of the behavior. These two parameters can be determined using data from the resonant column or bender element tests. In the absence of such data, one can use the tangent to the very beginning parts of stress-strain curves in triaxial tests. $H_1$, and $H_3$ (hardening parameters regarding radial shearing) can be determined using data from shear stress versus shear strain obtained from triaxial compression tests. Similarly, $H_2$ (hardening parameter under rotational shear) can be calculated by the results of shear strain *versus* the angle of principal stress axes rotation in the first cycle of principal stress axes rotation in rotational shear tests. Ignoring the small contribution of elastic strains, $D_1$ and $D_2$ (dilatancy parameters) can be determined using volumetric strain *versus* shear strain data obtained from the p-constant radial and the first cycle of principal stress axes rotation in pure rotational shear tests. $M_c$ and $M_e$ are the slopes of critical state line under compression and extension modes of triaxial in shear stress versus mean principal effective stress, q-p, plane. Also, by plotting data of critical state lines under compression and extension modes of triaxial in void ratio, e, *versus* mean

principal effective stress, p, plane, one can determine $e_A$, $\lambda$, $\xi$ (critical state line parameters), and an (anisotropy index) by the procedure explained in Dafalias et al. [39]. Alternatively, a can be determined by image analysis technique [10]. n and m are introduced in the model formulation in order to account for the effects of soil state on soil mechanical behavior. Once the location of the critical state line in the compression mode of the triaxial is determined, one can calculate n by $(-1/\psi)\ln(M_b/M_c)$, and m by $(1/\psi)\ln(M_d/M_c)$ at peak shear stress and phase transformation, respectively. $\chi$, a hardening parameter accounting for the densification effect under rotational shear can be determined using data from the produced shear and volumetric strain under the first and subsequent cycles of principal stress axes rotation. Finally, $f_0$, a parameter controlling the non-coaxiality of plastic flow can be determined when proper hollow cylindrical data on data of non-coaxiality angle *versus* stress ratio are available.

### *a) First set of comparisons*

Today, the triaxial test is very common in geotechnical engineering. Hence, the model capability is shown *versus* this mode of shear. Verdugo and Ishihara [4] published an extensive series of undrained experiments in the compression mode of triaxial on Toyoura sand samples prepared by the moist placement method. The tests cover a wide range of densities and stress levels. The model parameters used in simulations and their corresponding amounts are given in Table 2. It must be noted that in simulation of sand behavior subjected to the compression mode of triaxial, the model can be partially calibrated. In Figs. 4-6, comparisons between the model simulations and the experimental results of 11 undrained tests on dense $(e = 0.735, Dr \approx 64\%)$, medium loose $(e = 0.833, Dr \approx 38\%)$, and loose $(e = 0.907, Dr \approx 18\%)$ samples are shown. As seen, the model predictions match the experimental results, indicating the effectiveness of the model in the simulation of state dependent behavior of sand.

Table 2. Amounts of model parameters used in simulation of experiments reported by Verdugo and Ishihara [4]

| Elastic | Dilatancy | Plastic modulus | State parameter | Critical state line |
|---|---|---|---|---|
| $G_0 = 125^*$<br>$\nu = 0.15$ | $D_1 = 0.6$ | $H_1 = 2.5$<br>$H_3 = 1.0$ | $m = 3.5$<br>$n = 1.1$ | $M_c = 1.25$<br>$e_\tau = 0.934$<br>$\lambda = 0.019$<br>$\xi = 0.7$ |

*: $p_{ref}$ is taken 101 kPa

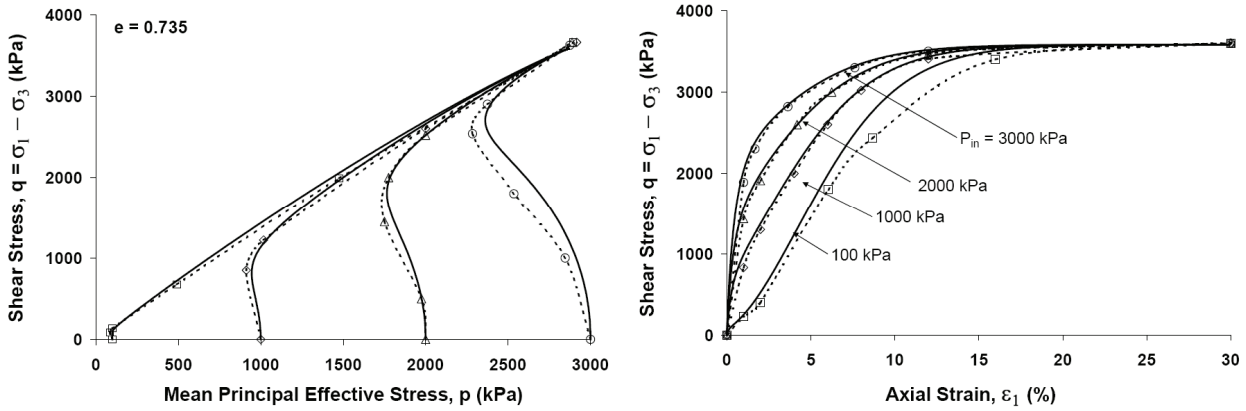


Fig. 4. The model predictions versus experiments for dense samples of Toyoura sand under triaxial compression (Data taken from Verdugo and Ishihara [4])

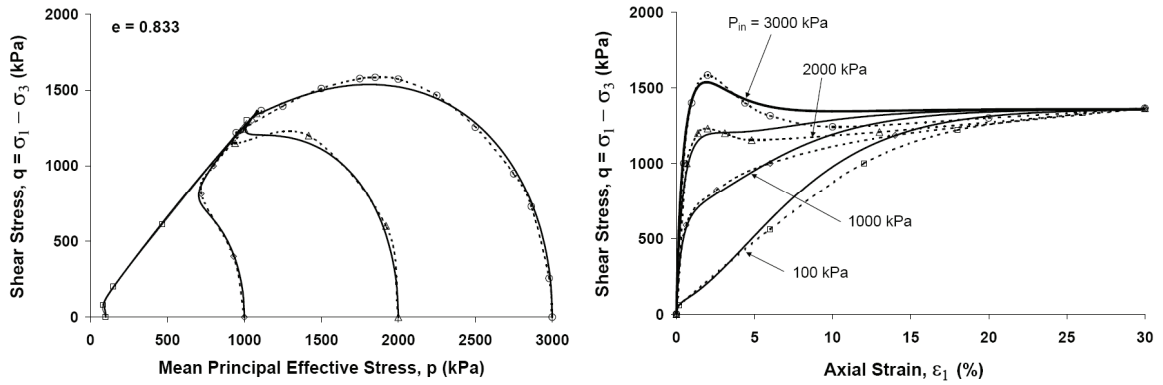


Fig. 5. The model predictions versus experiments for medium loose samples of Toyoura sand under triaxial compression (Data taken from Verdugo and Ishihara [4])

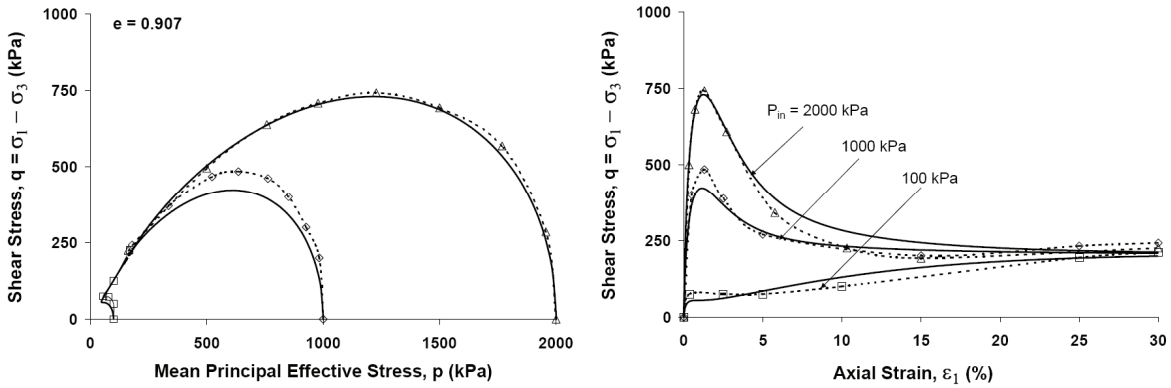


Fig. 6. The model predictions versus experiments for loose samples of Toyoura sand under triaxial compression (Data taken from Verdugo and Ishihara [4])

### *b) Second set of comparisons*

As stated before, sands exhibit drastic dependence of dilatancy and stiffness on the direction of applied loading with respect to the bedding plane. Using a hollow cylindrical apparatus, Yoshimine et al. [6] reported the results of 5 undrained tests on medium loose $(e = 0.821 - 0.828, Dr \approx 39 - 41\,\%)$ samples of Toyoura sand. Specimens were prepared by the dry deposition method which produces a different fabric from the fabric of samples prepared by moist placement. In the tests, after isotropic consolidation up to 100 kPa, samples were subjected to shear with different amounts of principal stress axes rotation along $\alpha$ = 15º, 30º, 45º, 60º, and 75º. The amounts of model parameters used for this set of simulation are listed in Table 3. In Fig. 7, the model predictions are compared with the experimental results. As seen from the comparisons, the model is able to consider the effect of anisotropy on the stress-strain behavior of sand when directions of principal stress axes were kept unchanged during loading.

Table 3. Amounts of model parameters used in simulation of experiments reported by Yoshimine et al. [6], Nakata et al. [9], and Yang et al. [11]

| Elastic | Dilatancy | Plastic modulus | State parameter | Critical state line | Anisotropy | Non-coaxiality |
|---|---|---|---|---|---|---|
| $G_0$= 125*<br>$\nu$ = 0.15 | $D_1$ = 0.5<br>$D_2$ = 0.4 | $H_1$ = 6.0<br>$H_2$ = 75.0<br>$H_3$ = 1.135<br>$\kappa$ =3.0 | m = 1.0<br>n = 1.3 | $M_c$ = 1.25<br>c = 0.75<br>$e_A$= 0.896<br>$\lambda$ = 0.019<br>$\xi$ = 0.7 | a = 0.278<br>$k_1$ = 0.15<br>$k_2$ = 0.65<br>$\chi$ = 1700.0 | $f_0$ = 20.0 |

*: $p_{ref}$ is taken 101 kPa

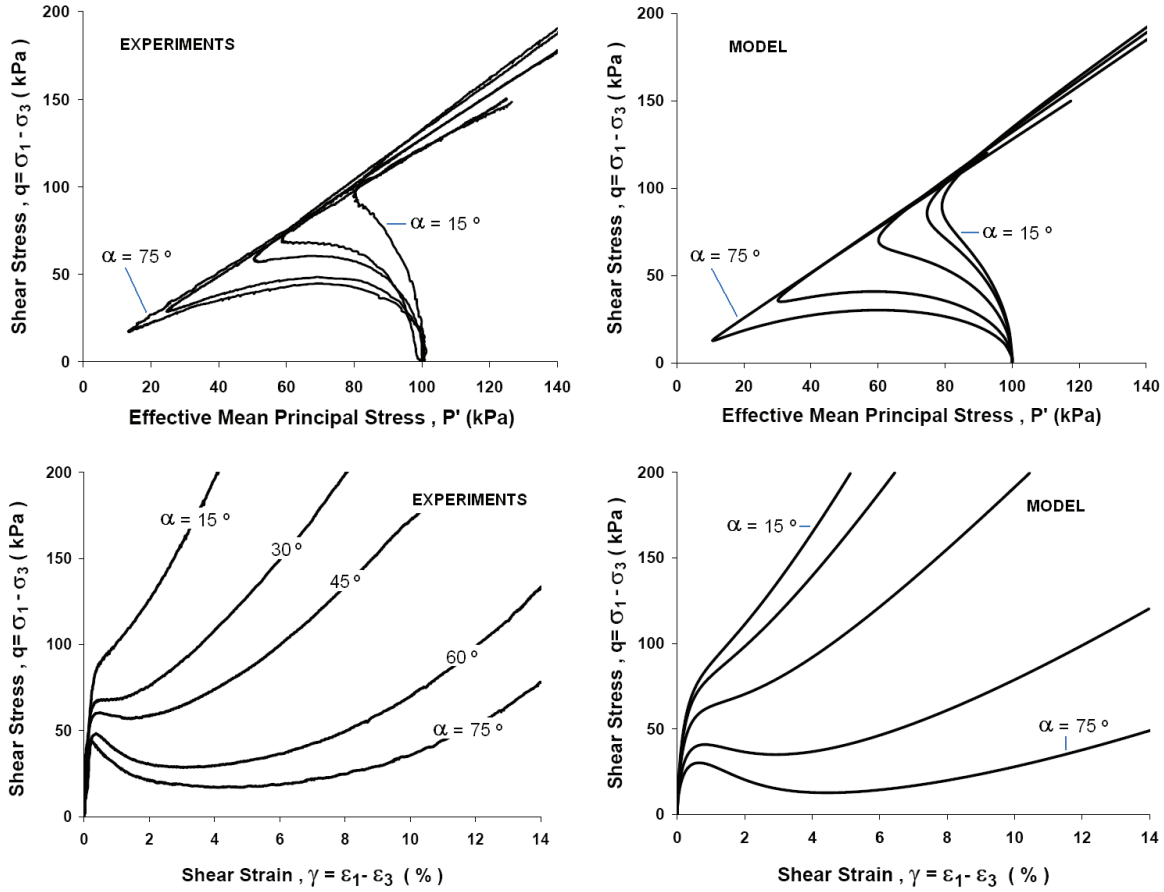


Fig. 7. The model predictions versus experiments on the effect of rotation of principal stress axes on sand behavior (Data taken from Yoshimine et al. [6])

### *c) Third set of comparisons*

Nakata et al. [9] published a work on the effect of rotation of principal stress axes on flow deformation of sand in a hollow cylindrical apparatus. A number of undrained rotational shear tests on dense and loose samples of Toyoura sand were reported in this paper. In the Nakata et al. [9] tests, samples were initially subjected to isotropic consolidation up to 100 kPa. Shear stress was then applied up to certain levels along $\alpha = 0°$. Finally, the directions of major and minor principal stress axes were rotated while the amount of shear stress was kept unchanged (Fig. 1). In Nakata et al. [9] the majority of rotational shear tests suffered from some internal instabilities manifested by large jump in stress paths and strain data. A set of comparisons using two samples that had no instabilities is conducted. Noting that samples were prepared by the dry deposition method, the parameters listed in Table 3 were used in simulations.

In Figs. 8 and 9, comparisons of model predictions and experimental results for strain components and developed pore water pressure (PWP) for two very dense $(e = 0.65, Dr \approx 90\%)$ and medium loose $(e = 0.85, Dr \approx 30\%)$ samples are presented.

### *d) Fourth set of comparisons*

More recently, Yang et al. [11] studied the effect of rotational shear on the undrained response of saturated Toyoura sand in a hollow cylindrical apparatus. All samples first were isotropically consolidated to mean principal effective stress of 100 kPa, and then were subjected to rotational shear under various amounts of shear stress defined as $q = \sqrt{[(\sigma_1 - \sigma_2)^2 + (\sigma_2 - \sigma_3)^2 + (\sigma_3 - \sigma_1)^2]/2}$ where b=0.5. Samples were prepared by dry deposition method. Therefore, the parameters given in Table 3 are used for

predictions. For three very dense and dense samples, comparisons of model simulations and the experiments for developed pore water pressure are shown in Fig. 10. In addition, Yang et al. [11] reported the normalized stress path of the sample with e=0.707 and q= 34.65 kPa. The model prediction corresponding to this test is compared with the experimental result in Fig. 11. As illustrated, the model is quite accurately able to predict the behavior of this set of experiments without any change of parameters.

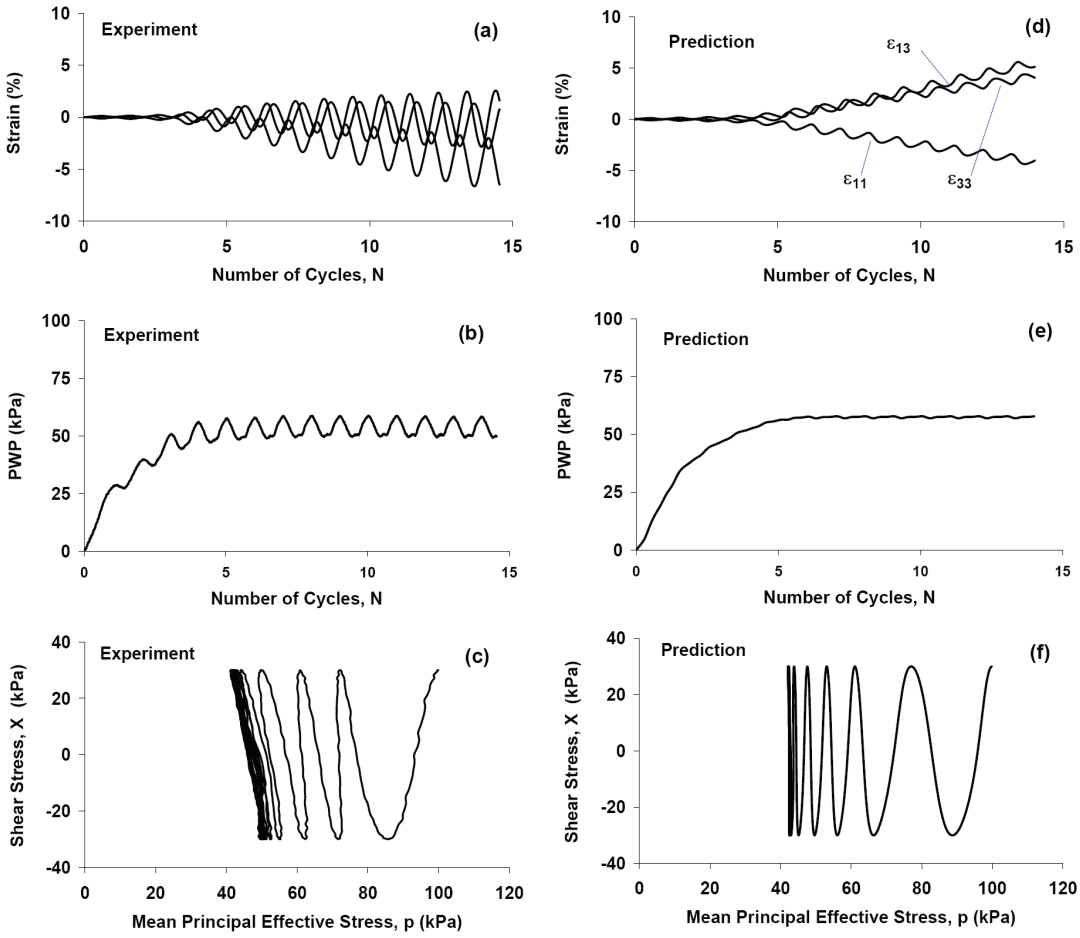


Fig. 8. The model predictions versus experiments on the effect of rotational shear on a very dense (e=0.65) sample of Toyoura sand: (a) and (d) developed strains; (b) and (e) developed pore water pressure; (c) and (f) shear stress versus mean principal effective stress (Data taken from Nakata et al. [9])

### *e) Parametric studies*

This section is organized to investigate the effect of parameter variation on the presented model simulations and sensitivity of results. It must be noted that the same parametric studies for samples subjected to radial drained and undrained paths can be found in other works of the author [23, 33]. Thus, parametric studies under rotational shear that were not considered in the previous works are only considered here. Effects of parameter variation on developed pore water pressure, and deviator strain for a sample within e=0.65 (the sample shown in Fig. 8) are illustrated in Figs. 12 and 13. It is worth mentioning that the parameters given in Table 3 were used as a reference in the simulations.

The presented parametric studies facilitate the parameter selection in obtaining the desired response for other granular media.

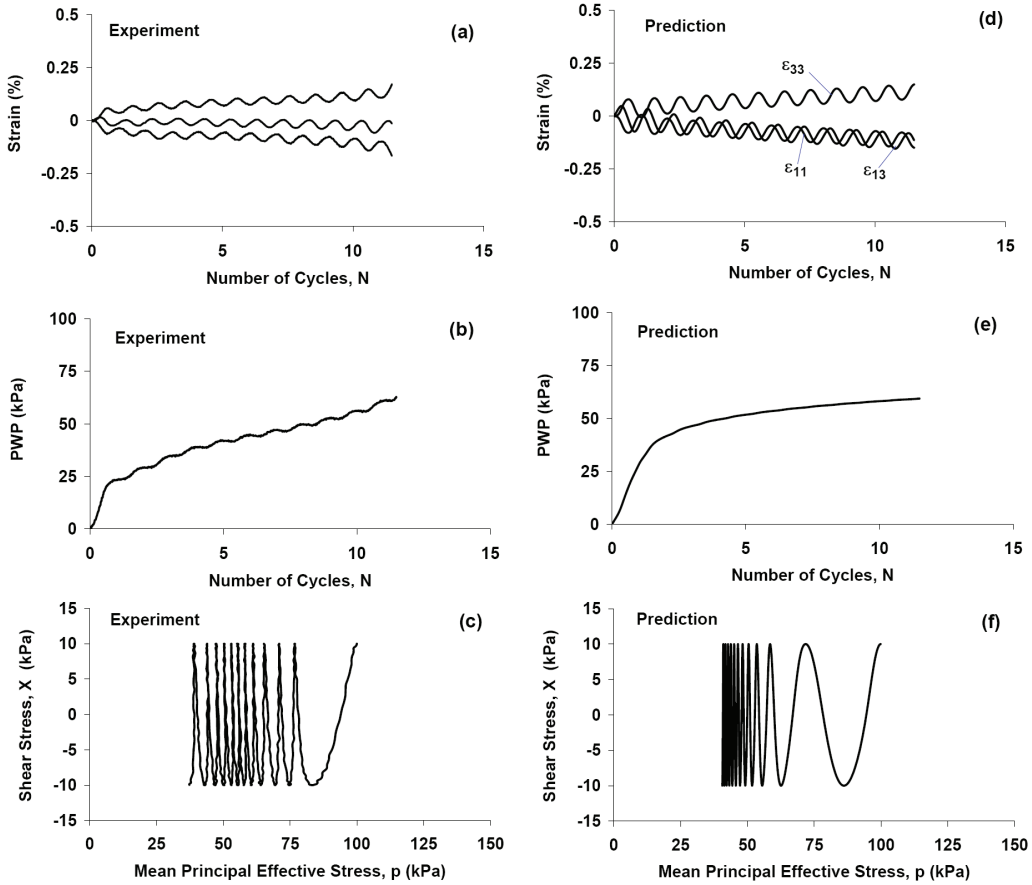


Fig. 9. The model predictions versus experiments on the effect of rotational shear on a medium loose sample (e=0.85) of Toyoura sand: (a) and (d) developed strains; (b) and (e) developed pore water pressure; (c) and (f) shear stress versus mean principal effective stress (Data taken from Nakata et al. [9])

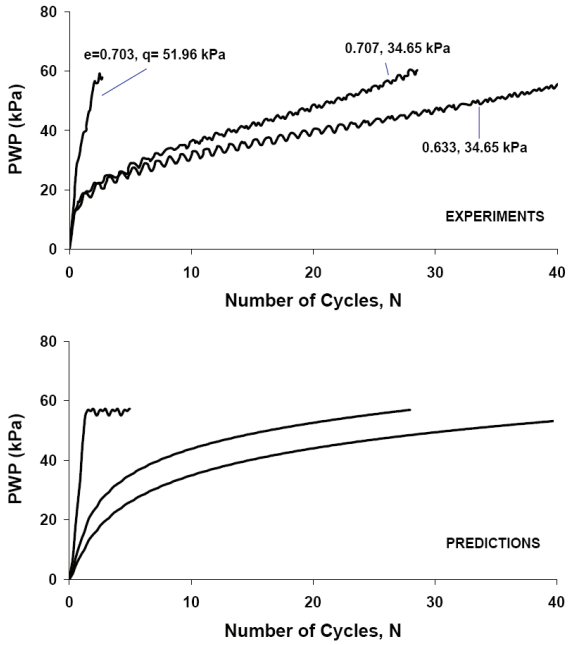


Fig. 10. Comparisons of model predictions versus experiments on pore water pressure developed in rotational shear under various conditions (Data taken from Yang et al. [11])

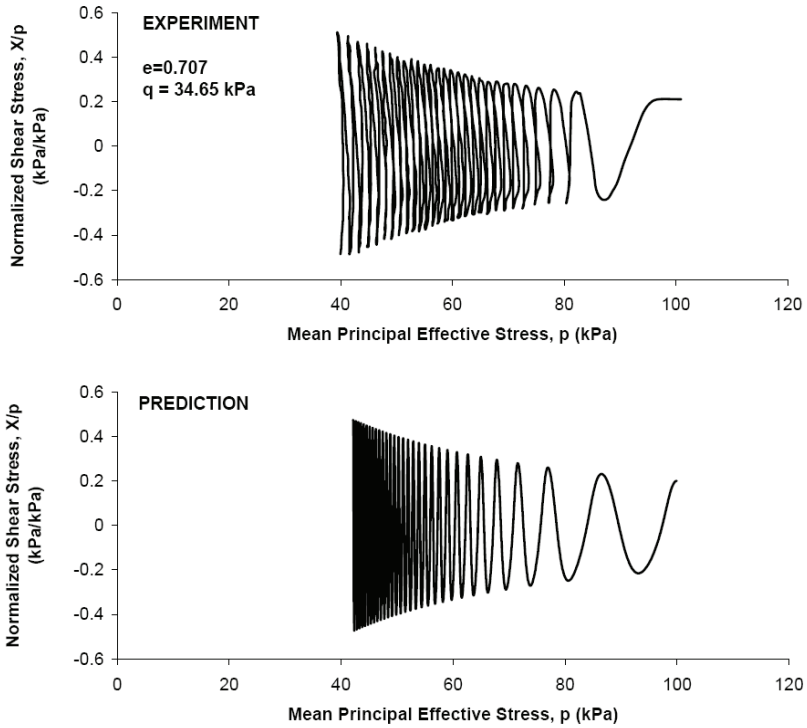


Fig. 11. Normalized stress path in X-p plane predicted by the model versus measured result (Data taken from Yang et al. [11])

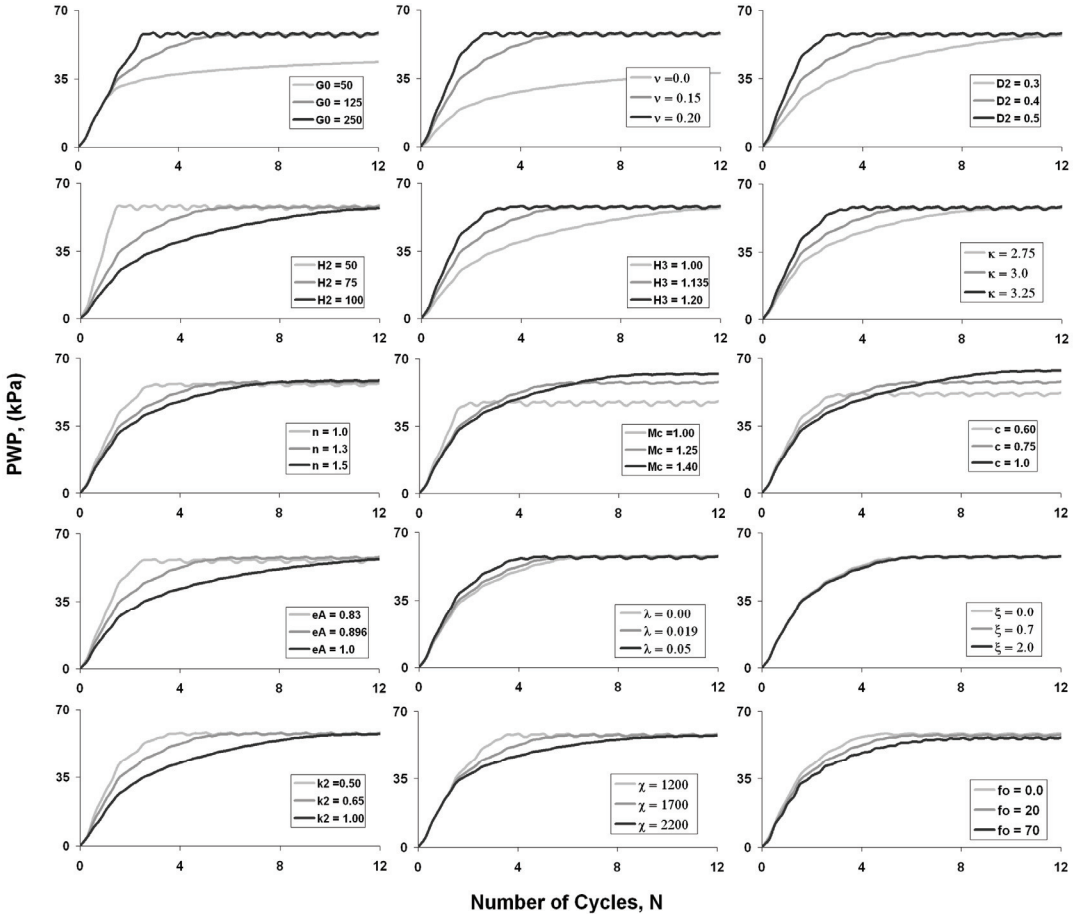


Fig. 12. Parametric studies of developed pore water pressure (PWP) versus cycles of principal stress axes rotation under undrained rotational shear

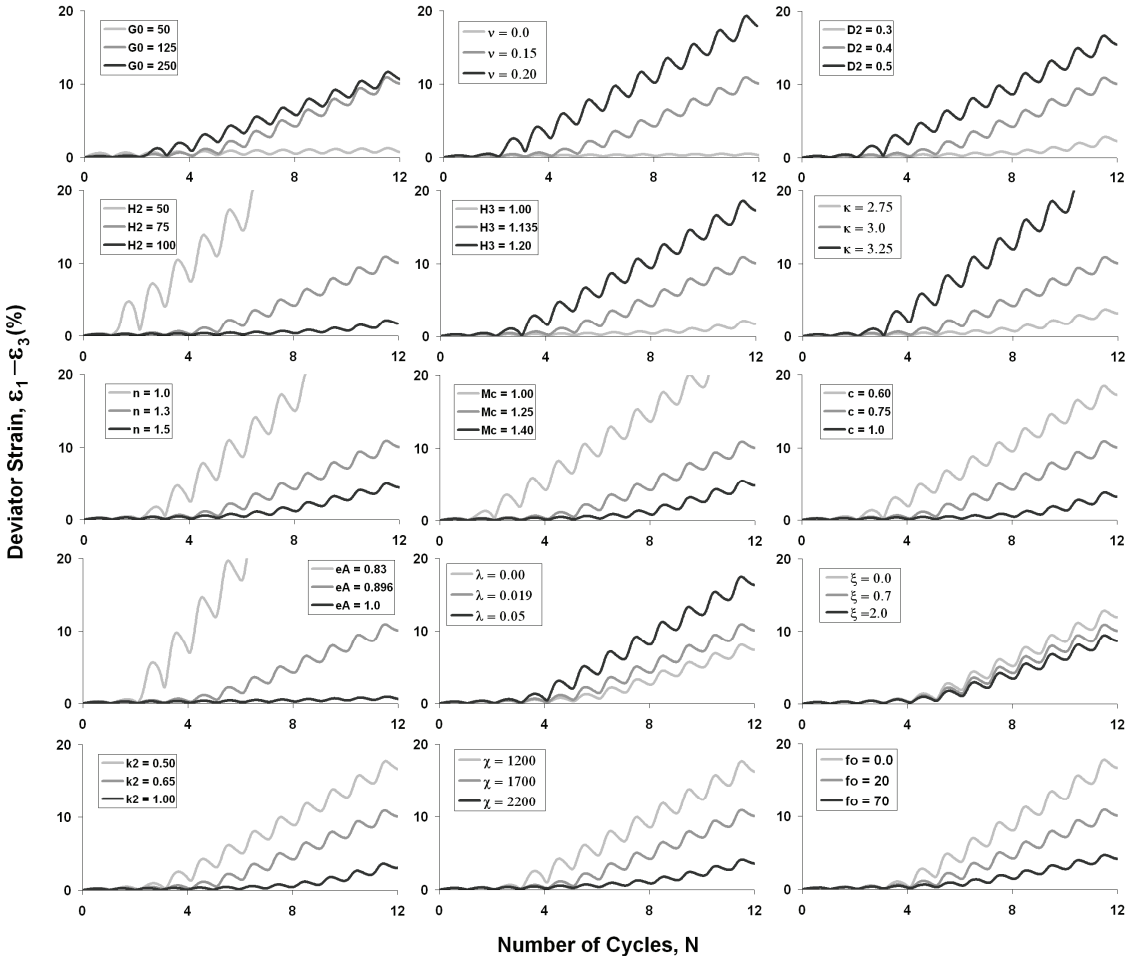


Fig. 13. Parametric studies of deviator strain, $\gamma = \varepsilon_1 - \varepsilon_3$, versus cycles of principal stress axes rotation under undrained rotational shear

## 7. CONCLUDING REMARKS

Within the context of bounding surface plasticity, a critical state compatible constitutive model is introduced. The presented model is able to account for the effect of soil state and fabric anisotropy on the mechanical behavior of sand subjected to shear under various stress paths including rotational shear. The first capability, state dependency, has been achieved by relating dilatancy and bounding surface size on the soil state represented by the state parameter of Been and Jefferies [1]. Accounting for soil anisotropic behavior, the second capability has been achieved by definition of some ingredients of the model as direct functions of two anisotropy state parameters. The model capability is validated using the experimental data of independent research groups. It has been shown that the model has quite a good capability in the simulation of liquefaction under rotational shear. It has also been demonstrated that for a particular preparation method, i.e. a particular fabric, the model is able to simulate sand behavior subjected to loading in various stress paths by using only one set of model parameters.

In the model formulation, it is assumed that the rotation of principal stress axes only takes place in the X-Y plane. This means that for more complex problems, further development of the model is essential. As a result, in its current form, the presented model can be used in practice for the analysis of 2-D geomechanical problems such as the bearing capacity and settlement of strip footing, and also the stability and deformation of long retaining walls, excavations, and embankments.

***Acknowledgements:*** The author wishes to thank Mr. Ehsan Seyedi Hosseininia for review of the manuscript. Dr. Mitsutoshi Yoshimine of Tokyo University and Dr. Yukio Nakata of Yamaguchi University Kindly provided the digital data of their experiments on Toyoura sand using HCA. Their kindness is appreciated.

## REFERENCES

1. Been, K. & Jefferies, M. G. (1985). A state parameter for sands. *Géotechnique*, Vol. 35, No. 2, pp. 99-112.
2. Been, K., Jefferies, M. G. & Hachey, J. (1991). The critical state of sand. *Géotechnique*, Vol. 41, No. 3, pp. 365-381.
3. Ishihara, K. & Towhata, I. (1983). Sand response in cyclic rotation of principal stress directions as induced by wave loads. *Soils and Foundations*, Vol. 23, No. 4, pp. 11-26.
4. Verdugo, R. & Ishihara, K. (1996). Steady state of sandy soils. *Soils and Foundations*, Vol. 36, No. 2, pp. 81-91.
5. Zlatović, S. & Ishihara, K. (1997). Normalized behavior of very loose non-plastic soils: effect of fabric. *Soils and Foundations*, Vol. 37, No. 4, pp. 47-56.
6. Yoshimine, M., Ishihara, K. & Vargas, W. (1998). Effect of principal stress direction and intermediate principal stress on undrained shear behavior of sand. *Soils and Foundations*, Vol. 38, No. 3, pp. 179-188.
7. Riemer, M. F. & Seed, R. B. (1997). Factors affecting apparent position of steady-state line. *ASCE J. Geotech. Geoenviron. Engng.*, Vol. 123, 3, pp. 281-288.
8. Uthayakumar, M. & Vaid, Y. P. (1998). Static liquefaction of sands under multiaxial loading. *Canadian Geotechnical Journal*, Vol. 35, pp. 273-283.
9. Nakata, Y., Hyodo, M., Murata, H. & Yasufuku, N. (1998). Flow deformation of sands subjected to principal stress rotation. *Soils and Foundations*, Vol. 38, No. 2, pp. 115-128.
10. Yang, Z. X., Li, X. S. & Yang, J. (2008). Quantifying and modeling fabric anisotropy of granular soils. *Géotechnique*, Vol. 58, No. 4, pp. 237-248.
11. Yang, Z. X., Li, X. S. & Yang, J. (2007). Undrained anisotropy and rotational shear in granular soil. *Géotechnique*, Vol. 57, No. 2, pp. 371-384.
12. Towhata, I. & Ishihara, K. (1985). Modeling soil behavior under principal stress axes rotation. *5th Int. Conf. on Numerical Methods in Geomechanics*, pp. 523-530, Japan.
13. Gutierrez, M., Ishihara, K. & Towhata, I. (1993). Model for the deformation of sand during rotation of principal stress directions. *Soils and Foundations*, Vol. 33, No. 3, pp. 105-117.
14. Sassa, S. & Sekiguchi, H. (2001). Analysis of wave-induced liquefaction of sand beds. *Géotechnique*, Vol. 51, No. 2, pp. 115-126.
15. Pastor, M., Zienkiewicz, O. C. & Chan, A. H. C. (1990). Generalized plasticity and the modeling of soil behavior. *International Journal for Numerical and Analytical Methods in Geomechanics*, Vol. 14, pp. 151-190.
16. Tsutsumi, S. & Hashiguchi, K. (2005). General non-proportional loading behavior of soils. *International Journal of Plasticity*, Vol. 21, pp. 1941-1969.
17. Chang, K. T. & Sture, S. (2006). Microplane modeling of sand behavior under non-proportional loading. *Computers and Geotechnics*, Vol. 33, pp. 177-178.
18. Sadrnejad, S. A. (2007). A general multi-plane model for post liquefaction of sand. *Iranian Journal of Science & Technology, Transaction B: Engineering*, Vol. 31, No. B1, pp. 123-141.
19. Li, X. S. & Dafalias, Y. F. (2002). Constitutive modeling of inherently sand behavior. *ASCE J. Geotech. Geoenviron. Engng*., pp. 128, No. 10, pp. 868-880.
20. Li, X. S. & Dafalias, Y. F. (2004). A constitutive framework for anisotropic sand including non-proportional loading. *Géotechnique*, Vol. 54, No. 1, pp. 41-55.

21. Lashkari, A. & Latifi, M. (2005). Modeling of non-coaxiality in granular materials via an anisotropy state variable. *Joint ASME/ASCE/SES Conference on Mechanics and Materials*, June 1-3, Baton Rouge, Louisiana, USA.
22. Lashkari, A. & Latifi, M. (2007). A simple plasticity model for prediction of non-coaxial flow of sand. *Mechanics Research Communications*, Vol. 34, No. 2, pp. 191-200.
23. Lashkari, A. & Latifi, M. (2008). A non-coaxial constitutive model for sand deformation under rotation of principal stress axes. *International Journal for Numerical and Analytical Methods in Geomechanics*, Vol. 32, No. 9, pp. 1051-1086.
24. Richart, F. E. Jr., Hall, J. R. & Wood, R. D. (1970). *Vibration of soils and foundations*. Englewood Cliffs. NJ: Prentice Hall.
25. Dafalias, Y. F. & Popov, E. P. (1975). A model of nonlinearly hardening materials for complex loadings. *Acta Mechanica*, Vol. 21, pp. 173-192.
26. Kreig, R. D. (1975). A practical two surface plasticity theory. *ASME J. Appl*. Mech., Vol. 97, pp. 641-646.
27. Hardin, B. O. (1978). 1-D strain in normally cohesionless soils. *ASCE J. Geotech. Engng*., Vol. 113, No. 12, pp. 1449-1467.
28. Thornton, C. (2000). *Microscopic approach contribution to constitutive modeling, In: Constitutive modeling of granular materials*. D. Kolymbas, ed., Springer, Berlin, pp. 193-208.
29. Wood, D. M. (2004). Experimental Inspiration for kinematic hardening soil models. *ASCE J. Engng. Mech*., Vol. 130, No. 6, pp. 656-664.
30. Gudehus, G. (1973). Elastoplastic stoffgleichungen fur trockenen sand. *Ingenieur-Archiv*. Vol. 42, pp. 151-169.
31. Li, X. S. & Dafalias, Y. F. (2000). Dilatancy for cohesionless soils. *Géotechnique*, Vol. 50, No. 4, pp. 449-460.
32. Oda, M. & Nakayama, H. (1989). A yield function for soils with anisotropic fabric. *ASCE J. Mechanics of Materials*, Vol. 115, pp. 89-104.
33. Lashkari, A. (2007). A constitutive model for non-coaxial flow of sand. *PhD Thesis, University of Tehran*.
34. Vardoulakis, I. & Georgopoulos, I. O. (2005). The "stress-dilatancy" hypothesis revisited: shear-banding related instabilities. *Soils and Foundations*, Vol. 45, No. 2, pp. 61-76.
35. Miura, K., Miura, S. & Toki, S. (1986). Deformation behavior of anisotropic dense sand under principal stress axes rotation. *Soils and Foundations*, Vol. 26, No. 1, pp. 36-52.
36. Ishihara, K., Tatsuoka, F. & Yasuda, S. (1975). Undrained deformation and liquefaction of sand under cyclic stresses. *Soils and Foundations*, Vol. 15, No. 1, pp. 29-44.
37. Vaid, Y. P. & Chern, J. C. (1985). Cyclic and monotonic undrained response of saturated sands. *Proceedings of, Advances in the Art of Testing Soils under Cyclic Loading*, ASCE, New York, pp. 120-147.
38. Mooney, M. A., Finno, J. & Viggiani, M. G. (1998). A unique critical state for sand? *ASCE J. Geotech. Geoenviron. Engng*., Vol. 124, No. 11, pp. 1100-1108.
39. Dafalias, Y. F., Papadimitriou, A. G. & Li, X. S. (2004). Sand plasticity model accounting for inherent fabric anisotropy. *ASCE J. Engng. Mech.*, Vol. 130, No. 11, pp. 1319-1333.
40. Gutierrez, M., Ishihara, K. & Towhata, I. (1991). Flow theory for sand during rotation of principal stress direction. *Soils and Foundations*, Vol. 31, 4, pp. 121-132.